PCCP

Accepted Manuscript

ROYAL SOCIETY OF CHEMISTRY

www.rsc.org/pccp

Molecular structure and stability of dissolved lithium polysulfide species

M. Vijayakumar, Niranjan Govind, Eric Walter, Sarah D Burton, Anil Shukla, Jie Xiao, Jun Liu, Chongmin Wang and S. Thevuthasan*

Graphical Abstract:

We present a molecular level study of dissolution mechanism and subsequent chemical stability of lithium polysulfide species using combined experimental and theoretical approach.

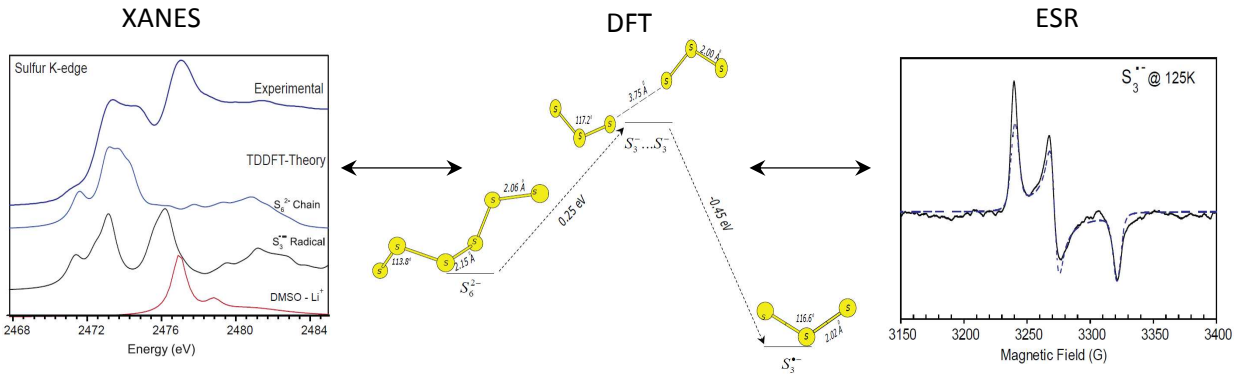

PCCP

RSCPublishing

ARTICLE

Molecular structure and stability of dissolved lithium polysulfide species

Cite this: DOI: 10.1039/x0xx00000x

M. Vijayakumar, Niranjan Govind, Eric Walter, Sarah D Burton, Anil Shukla, Arun Devaraj, Jie Xiao, Jun Liu, Chongmin Wang, Ayman Karim and S. Thevuthasan*

Revised 27th January 2014,

ID: EE-ART-12-2013-043994

DOI: 10.1039/x0xx00000x

www.rsc.org/

Ability to predict the solubility and stability of lithium polysulfide is vital in realizing longer lasting lithium-sulfur batteries. Herein we report combined experimental and computational analyses to understand the dissolution mechanism of lithium polysulfide species in an aprotic solvent medium. Multinuclear NMR, variable temperature ESR and sulfur K-edge XAS analyses reveals that the lithium exchange between polysulfide species and solvent molecule constitutes the first step in the dissolution process. Lithium exchange leads to de-lithiated polysulfide ions (S_n^{2-}) which subsequently forms highly reactive free radicals through disproportion reaction ($S_n^{2-} \longrightarrow 2S_{n/2}^{\bullet -}$). The energy required for the disproportion and possible dimer formation reactions of the polysulfide species are analyzed using density functional theory (DFT) based calculations. Based on these findings, we discuss approaches to optimize the electrolyte in order to control the polysulfide solubility.

Broad Impact

Sulfur is a promising cathode for high energy density lithium-sulfur battery, but plagued by polysulfide dissolution and parasitic reaction which limits their cycling performance. Despite intensive efforts to design optimal materials to overcome these drawbacks, the progress in this field has been slow due to the fundamental gap in understanding of the polysulfide dissolution mechanism and their parasitic reactions. Herein, we report a molecular level study of the dissolution mechanism and subsequent formation of highly reactive free radicals from dissolved polysulfide species using a combined experimental and theoretical approach. This work will provide the necessary insight for the rational and optimal design of materials for lithium-sulfur batteries.

1 Introduction

The growing energy demand to power modern technologies ranging from portable electronic devices to large scale electrical grids has fueled research towards the development of high energy density batteries. In this regard, lithium-sulfur (Li-S) and flow type lithium-polysulfide (Li-PS) batteries have emerged as promising candidates for portable and large scale energy storage respectively[1, 2]. These batteries offer economic and environmental advantages as the sulfur based cathode/catholyte materials are environmentally benign and naturally abundant[3, 4]. Despite these attractive attributes, sulfur based materials pose significant challenges. For example, the sulfur cathode in Li-S batteries have inherent material challenges such as, enormous volume changes upon lithium cycling, poor conductivity and

dissolution of lithium sulfides in organic electrolytes during electrochemical process[4]. These issues result in rapid capacity loss during the charge/discharge cycles and thereby hamper the life cycle of the battery. Among these challenges, the volume expansion and low conductivity of the sulfur cathode have been elegantly dealt with carbon based nano-structural designs such as sulfur encapsulated in carbon/graphene spheres[5-8]. These novel approaches provide the necessary electronic conductivity and "*cushioning*" to mitigate the huge volume changes during the cycling process. However, dissolution of lithium polysulfide (Li_2S_n) in the electrolyte is still a major challenge which hampers progress. Dissolution leads to the so-called "*shuttle phenomenon*" where the polysulfide molecules diffuse to the lithium negative electrode and causes dendrite growth through parasitic reactions[9]. Since these reactions occur repeatedly during the cycling process, this in turn significantly reduces the charge/discharge capacity of the Li-S cell. Similarly, the flow type lithium polysulfide cell can form unstable lithium polysulfide species during operation which can cause precipitation and/or parasitic reactions during charge/discharge process. Briefly, the dissolved polysulfide species and their chemical reactivity during the cycling operation is the origin for most of the issues encountered in sulfur based batteries[10].

In recent years multiple strategies have been employed to address the "*shuttle phenomenon*" and increase the life cycle of the Li-S battery. Some of the popular approaches are, designing an optimal electrolyte which can resist the high solubility of lithium polysulfides[11], placing a carbon membrane to act as a physical barrier to block the polysulfide species[12-15], coating the electrode materials with protective layers or additives to prevent parasitic reactions with the polysulfide species[16, 17] and employing porous materials as internal reservoirs which can absorb/desorb polysulfides during electrochemical cycling[18]. Despite these attempts, achieving extended cycling (>500 cycles) with minimal capacity loss for both Li-S and Li-PS batteries still poses a significant challenge[19]. This difficulty stems mainly from the big gap in understanding that exists between battery material synthesis efforts and fundamental studies about the molecular structure and stability of dissolved polysulfide species. In particular, molecular level insight about the dissolution mechanisms of polysulfide species and their chemical stability within organic solvents is still unclear. This hampers the rational design of electrolytes, coatings and reservoir materials. Similarly, designing a solvent system to enhance higher solubility and electrochemical stability is essential for flow type Li-PS batteries. Therefore, exploring the dissolution mechanisms and stability of polysulfide species from a molecular standpoint is vital for the development of longer lasting Li-S and flow type Li-PS batteries.

Interestingly, sulfur has a large number of allotropes and forms a wide range of lithium polysulfides (Li_2S_n, $1 \leq n \leq 8$) during battery operation. Thus far, research efforts have mainly been focused on analyzing the electrochemical behavior of polysulfide species and/or identifying the polysulfide intermediate species formed during the Li-S battery cycling process[9, 11, 20, 21]. In particular, multiple polysulfide species with different sulfur chain-lengths ($1 \leq n \leq 8$) and radical anions ($S_3^{\bullet-}$) due to possible reversible disproportionation reactions have been reported[20]. These studies shed light on possible intermediate polysulfide species formed during the charge/discharge cycles. For example, recent analytical studies have reported that, among the many polysulfide species, Li_2S_n ($4 \geq n \leq 8$) are the most frequently formed intermediates during the battery cycle conditions[22]. In addition, the possibility of polysulfide cluster formation such as $(Li_2S_n)_x$ (x=1,2,3 or 4) in electrolyte solutions have also been postulated computationally[23]. Despite these attempts, the molecular structure and stability of these lithium polysulfide species are still unclear. In this paper, we combine experimental spectroscopic studies (magnetic resonance, X-ray absorption spectroscopy) with density functional theory (DFT) calculations to shed light on the dissolution mechanisms and chemical stability of polysulfide species.

2. Experimental Section

2.1 Choice of solvent system: Since traditional polycarbonate based lithium battery electrolytes are chemically reactive with polysulfide species[24, 25], 1,3-dioxolane (DOL) and/or Dimethoxy ethane (DME) based electrodes are generally used in Li-S battery[26]. These DOL and/or DME based electrolytes are polar - aprotic solvents which yields higher solubility for polar molecules such as polysulfide[27]. However, these solvent systems have poor thermal stability which can pose serious limitations in variable temperature molecular spectroscopy analysis. Hence, DMSO is an ideal choice, which is a similar polar aprotic solvent, and is also known to host stable polysulfide species over wide temperature range [28, 29]. This relatively higher thermal stability of DMSO is ideal for the variable temperature spectroscopic measurements which is crucial for analyzing the energy profile of polysulfide molecules. Similarly, the presence of well-studied sulfonyl group in the DMSO acts as internal reference for both NMR and XAS spectroscopic measurements (will be discussed later). Finally, the molecular structure of polysulfide species in DMSO solvent derived using combined theoretical and experimental approach were compared with computationally derived polysulfide structure with DOL and DME (1:1) solvent system. The similarities in the polysulfide molecular structure confirms the validity of DMSO as model solvent system (will be discussed later).

2.2 Synthesis Lithium polysulfides are synthesized by a solution chemistry method as reported in the literature [28]. Briefly, stoichiometric amounts of Lithium sulfide (Li_2S) and elemental sulfur (S) were mixed and stirred for 12 hours in dimethyl sulfoxide (DMSO) [28]. Two solution samples **A** and **B** with target compositions of Li_2S_4 and Li_2S_6 were prepared. The choice of these lithium polysulfide molecules is based on recent reports [1, 2, 20, 26] that have identified them as the major intermediate phase that is formed in both Li-S and Li-PS batteries. This is mostly likely due to their higher solubility[1, 2, 22, 30]. However, dissolved polysulfide ions are more likely to produce a phase mixture in solution thereby providing a spectrum of polysulfide species[31-33]. In fact our attempts to prepare a Li_2S_8 solution sample yielded a phase mixture of Li_2S_6 possibly due to the dissociation reaction $S_8^{2-} \longleftrightarrow \frac{1}{4}S_8 + S_6^{2-}$ in organic solvents[34, 35]. The sample preparation and subsequent packaging for experimental measurements were performed in an inert atmosphere to avoid possible oxidation of the polysulfide molecules into thiosulfates[36].

2.3 Mass Spectroscopy Measurements Mass spectrometry (MS) analyses of the samples were performed by electro-spraying the diluted solutions (10x in DMSO) from an etched silica capillary emitter (150 micron OD x 20 micron ID) at a flow rate of 1 microliter/minute and floating the metal union at 2.2 kV. The ESI tip was placed at a distance of ~3 mm from a 580 micron ID heated capillary interface (200^o C) to an Exactive mass spectrometer (Thermo Fisher Scientific). In the positive ion mode, clusters of DMSO-Li^+ dominate the spectrum but no polysulfide cations were observed related to Li_2S_n. However, operating the mass spectrometer in the negative ion mode by reversing polarities of all necessary voltages for electrospray and ion transmission, several anions with different combinations of polysulfide species were observed. All the mass spectra were recorded at a mass resolution of 25000.

2.4 Magnetic Resonance Measurements The electron paramagnetic resonance (EPR) spectra were performed using a Bruker Elexsys 580 spectrometer fitted with a SHQE resonator and a continuous nitrogen flow variable temperature insert. Samples were contained in small diameter (1.5mm o.d. x 1 mm i.d.) Teflon tubes which were then sealed in conventional 4*mm* x 3*mm* Quartz EPR tubes. Microwave frequency was ~9.3 GHz (X band) at 20 mW power. The field was swept 1200 G in 167 s for spectra recorded at room temperature and above, and 300 G in 20 s for the 125 K spectrum. The field was modulated at a frequency of 100 kHz at 1 G amplitude. A time constant of 163 ms was employed. The variable temperature spectra were obtained by programming the temperature controller to increase the temperature in a ramp of 5 Kelvin steps, the sample was allowed to equilibrate at each step, and the actual

temperature was recorded at the time of the spectrum. The concentration of the free radicals were calculated using spin-counting method, where the acquired peak integrals are compared with peak integrals of known quantity of nitroxide free radical in 2,2,6,6-tetramethylpiperidine-N-oxide (TEMPO) solution. The ^{6}Li and ^{17}O nuclear magnetic resonance (NMR) measurements were done with natural abundance (*i.e.* without any isotope enrichments) using Varian 500 Inova spectrometer (B_0=11.1T; ^{6}Li and ^{17}O Larmor Frequencies are 73.58 and 67.8 MHz respectively). All NMR measurements were carried out using 5*mm* standard NMR glass tube with Single pulse sequence under room temperature (~24°C) condition. The observed ^{6}Li and ^{17}O chemical shifts were externally referenced (δ_{iso} = 0 *ppm*) to 1M aqueous LiCl solution and natural abundance D_2O solution respectively.

2.5 X-ray Absorption Spectroscopy Sulfur K-edge x-ray absorption near-edge spectroscopy (XANES) measurements were performed at the National Synchrotron Light Source (NSLS) beam line port X-19A. The first resonance (white line) of sulfur powder (2472.5 eV) was used as the standard reference for energy calibration. Subsequently, spectra were recorded for polysulfide solutions and pure DMSO which were separately packed in a polyimide tube (ID ~ 2mm and thickness ~ 16 microns) and sealed with epoxy resins. The scan step size was 0·6 eV in the pre-edge region between 2350 and 2480 eV, 0·09 eV between 2460 and 2490 eV, the main region of interest, and 0·2 eV between 2490 and 2510 eV. Typical integration times were 500–1000 ms per point. A linear background determined in the pre-edge region was subtracted from the raw data to correct the absorption from higher shells and from supporting materials.

2.6 Computational Methods Ground state density functional theory (DFT) based calculations were carried out using the *Amsterdam Density Functional* (ADF-2013) package[37]. The hybrid-GGA based Becke, three-parameter, Lee-Yang-Parr (B3LYP) exchange-correlation functional with dispersion correction (DFT-D3) was employed for geometry calculations [38-41]. All the calculations reported herein were carried out using the TZ2P basis set (triple *Z*, double polarization function, all electron) with the Slater type functional implemented in the ADF program. As a first step, we considered gas phase molecular structures of Li_2S_n without any geometrical constraints, which were subsequently used as seed structures to construct a supramolecular structure where it is surrounded by six explicit DMSO solvent molecules. This supramolecular structure was again fully optimized using the COSMO model with DMSO as solvent to fully capture the solvent induced structural conformations. Molecular structures optimized using this supramolecular setup were used for all the spectroscopy and reaction energy

calculations. NMR chemical shift calculations were performed with three different DFT functionals (BLYP, PBE and B3LYP) to assess the errors in the calculations. The ^{6}Li and ^{17}O chemical shifts were calculated at fully optimized geometry and referenced with respect to hydrated Li+ *i.e.* $[Li.(4H_2O)]^{+}.Cl^{-}.6H_2O$ and a cluster of DMSO molecules, respectively. This is representative of the aqueous LiCl and DMSO solvents commonly used as external references in experimental NMR spectroscopy measurements. Sulfur K-edge near edge X-ray absorption (XANES) calculations were performed using a linear response time-dependent density functional theory (LR-TDDFT) based approach as implemented in the NWChem quantum chemistry program[42-46]. Scaled ZORA eigenvalues were used to account for relativistic effects in the core excitation energies[47, 48]. All XANES calculations were performed with the Sapporo-TZP-2012 basis[49, 50] for Li and S, the 6-31G* basis[51, 52] for C and O and the 3-21G basis [51, 52] for H and the BHLYP exchange-correlation[40, 53], respectively.

3. Results and Discussion

3.1 Speciation of lithium polysulfide molecules: During the dissolution process the elemental sulfur in the S_8 crown structure opens to form polysulfide chains of varying lengths *i.e.* S_n^{2-} *(n=1 to 8)*[54]. The di-radical sulfur atoms (S^{-}) at both ends of these nucleophile polysulfide ions (S_n^{2-}) can bond with lithium to form various types of lithium polysulfide species such as Li_2S_n *(n=1 to 8)*. In addition, recent analytical and computational studies have suggested that lithium polysulfide species might exist in cluster form $(Li_2S_n)_m$ (*m and n*=1 to 4) in electrolyte solutions. In particular, the Li_2S_4 and Li_2S_6 molecules that we focus on in this work can exist as dimer units such as Li_4S_8 and Li_4S_{12} via simple cluster formation, i.e. $2\left(Li_2S_n\right)\longrightarrow Li_4S_{2n}$. Therefore, we first analyzed the solutions **A** and **B** to identify the type of lithium polysulfide species in the solution. We carried out high resolution electro-spray ionization mass spectrometry (MS) analysis in both negative and positive ion modes. In the negative ion mode, the MS spectrum is dominated (>80%) by de-lithiated polysulfide species such as $S_3^{\bullet-}/S_6^{2-}$ (*m/z* = 95.916) and $S_2^{\bullet-}/S_4^{2-}$ (*m/z* = 63.944) along with notable amount (~10%) of lithium polysulfides LiS_n^{-} *(n=4,6, 8)* († Fig. S1). Similarly, low intensity peak (<5%) at *m/z* =276.824 of MS spectra shows the possible presence of $Li_3S_8^{-}$ a dimer type clustered polysulfide molecules in both **A** and **B** solutions. Interestingly, other possible dimer molecules such as $Li_3S_{12}^{-}$ are not detected in the solution within the detectable limit (~2%) of the spectrometer. On the other hand, the positive ion mode MS spectra are dominated by $(DMSO)_n$-Li^{+} molecules indicating the possible chemical interaction between lithium and DMSO solvent molecule († Fig. S2). Overall, our MS analysis indicates that both solutions **A** and **B** have phase mixtures consisting

mainly of de-lithiated polysulfide species (S_n^{2-}), lithium polysulfides (*i.e.* Li_2S_4, Li_2S_6 and Li_2S_8) and possibly small concentrations of clustered dimer-type molecules Li_4S_8 and Li_4S_{12}. However, it should be noted that the possibility of fragmentation due to higher voltage and temperature conditions used in electrospray MS makes it difficult to quantify the polysulfide species in the solution. Nevertheless, it is clear that our solutions mostly contain allotropes of lithium polysulfide species specific to Li_2S_4, Li_2S_6 and Li_2S_8. We shall only focus on these polysulfide species as part of our experimental and theoretical analysis.

3.2 Molecular structure of lithium polysulfide: To unravel the molecular structure of dissolved polysulfide species and the possibility of dimer formation, we carried out DFT based geometry optimizations using the supramolecular setup described earlier. Figure 1 shows monomer units of Li_2S_6 and Li_2S_8 molecules with the calculated bond lengths (explicit solvent molecules are not shown for clarity). It is interesting to note that these monomer units of lithium polysulfide molecules display varying S-S bond lengths ranging from 2.01Å to 2.39Å and have nonequivalent sulfur atoms within their chain structure. In particular, the higher order Li_2S_n ($n\geq6$) structures show wide variations in the S-S bond length, whereas the bond length is close to ~ 2.07±0.02 Å in the Li_2S_4 molecule which is the typical S-S bond length of polysulfide ions (S_n^{2-}). On the other hand, the optimized Li-S bond length (2.57±0.02 Å) in these lithium polysulfide molecules using the supramolecular setup is longer than the bond length (~2.35 Å) optimized in the gas phase (*i.e.* no solvent) as well as in a pure implicit solvent (COSMO) environment. The longer S-S and Li-S bonds suggest a decrease in bond energy and the possibility of bond scission which will be discussed later in detail.

To understand the possibility of lithium polysulfide cluster formation, we optimized both monomer units and their respective dimer units (*i.e.* Li_4S_{2n}). Cluster formation can proceed through simple sharing of lithium cations between two monomer units as follows $2(Li_2S_n)xDMSO \longrightarrow (Li_4S_{2n}).2xDMSO$. Figure 2a shows the molecular structure of Li_4S_8 which is the dimer form of Li_2S_4 optimized with the supramolecular setup. Similar to its parental monomer unit, the Li_4S_8 molecule also has a S-S bond length of 2.09±0.02 Å indicating a relatively stronger bond. Although the other dimer forms (i.e. Li_4S_{12} and Li_4S_{16}) show slightly longer S-S bond lengths (2.20±0.02 Å), they are still below respective parental monomer units. However, all the dimer forms show a wide variation in the Li-S bond length (~2.32±0.25 Å) due to the increase in lithium coordination. This is not surprising considering that lithium acts as

bridging atom between the monomer units. To explore the possibility of dimer formation in DMSO solution we calculated the respective bonding energies. The bonding energy requirement for these cluster formation reactions are calculated as the difference between bonding energy of the product and reactant molecules with the supramolecular setup. The calculated energy for cluster formation for all three lithium polysulfide molecules (*i.e.* Li_2S_4, Li_2S_6 and Li_2S_8) are shown in Figure 2b. This predicts that the higher order polysulfides (*i.e.* with longer chain) such as Li_2S_8 are more likely to exist as monomer units in DMSO solutions. On the other hand, Li_2S_4 with its relatively shorter chain length favors dimer formation (Li_4S_8) in the DMSO solution. Interestingly, Li_2S_6 which is a common intermediate observed during battery operation only slightly favors dimer formation. However, it should be noted that this relatively smaller energy barrier (~0.25eV) is prone to solvent and thermally induced conformational changes which can tilt the cluster formation in either way. Overall, our calculations of the bonding energies are consistent with our MS analysis, where the dimer form of Li_4S_8 and monomer of Li_2S_6 are observed. We note that the moderate bonding energy differences calculated for lithium polysulfide molecules (*i.e.* Li_2S_4 and Li_2S_8) can be affected by thermal and solvent concentration effects and requires further analyses.

The structural stability and associated conformational changes of dissolved species are influenced by the free energy landscape determined by solute-solvent interactions and controlled by thermal kinetics. Any subsequent dimer formation in lithium polysulfide species could very well be solvent and temperature dependent. This result agrees with the smaller percentage (<3%) of dimer molecules observed in our MS analysis which is subject to high temperature conditions where molecular fragmentation is quite possible due to this moderate energy barriers between monomer and dimer units. Apart from the temperature effects, the solvent effects (such as nature of solvent molecule and relative concentration) can also play a crucial role on cluster formation in dissolved polysulfide species.

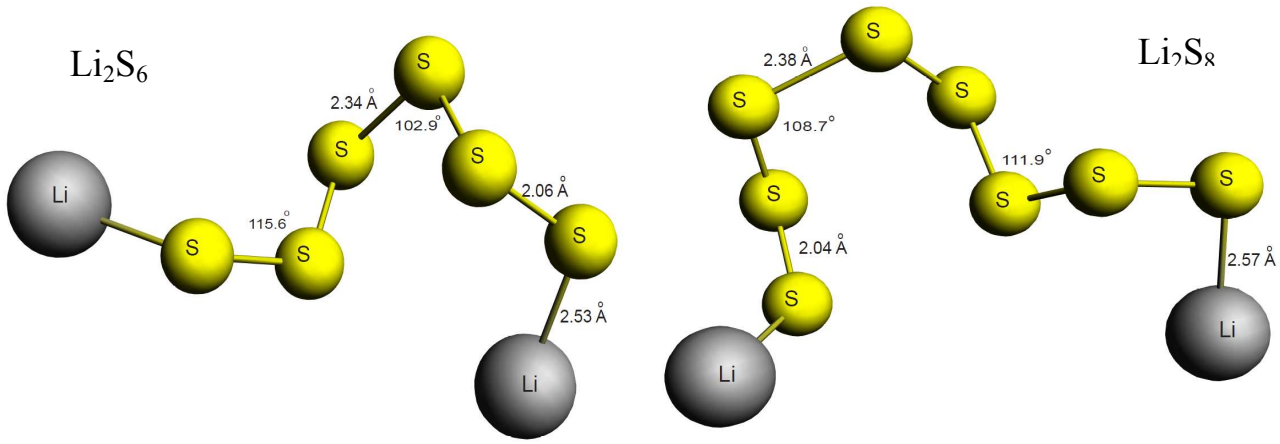

Figure 1. *Molecular structure of Li_2S_6 and Li_2S_8 monomer units optimized using B3LYP-D3 with all electron TZ2P basis sets. The sulfur and lithium atom are represented by yellow and gray spheres respectively. For clarity only the seed polysulfide molecule is shown. The supramolecular setup can found in the supplemental information section (Fig.S3).*

To further analyze the solvent effects, we also calculated the energy required for cluster formation by using a pure implicit solvent model (*i.e.* COSMO with DMSO as solvent). With these models, the dimer forms of lithium polysulfide molecules (*i.e.* Li_4S_8, Li_4S_{12} and Li_4S_{16}) are energetically favorable irrespective of sulfur chain lengths by ~ 1.5±0.2eV. This result is in agreement with recent DFT results[23]. However, the discrepancy in the energy requirement for cluster formation with implicit and explicit solvent models emphasizes the importance of explicit solvent interactions in conjunction with conformational changes of the lithium polysulfide molecules. For example, in lithium polysulfide molecules, the lithium ions at the end of the sulfide chains can chemically interact with solvent molecules. The sulfonyl oxygen in DMSO (i.e. *S=O*) is slightly negatively charged (due to the dipolar character in its interaction with sulfur) and can potentially bond with lithium ions at the ends of the lithium polysulfide molecules. Such an interaction between Li and solvent molecule can directly impact the possible intermolecular Li-Li bonding between monomer units and subsequent dimerization (*i.e.* Li_4S_{2n}).These specific interactions are absent in implicit solvent models reported earlier[23]. Therefore supramolecular setup used in this study, which combines the implicit solvent model with explicit solvent molecules, is essential for the description of Li interaction with solvent molecule and predicting the polysulfide molecular structures. The Li interaction with solvent molecule also depends on polysulfide molecular structure, as evident in gradual increase in Li-S bond length and subsequent decrease in Li-O bond length with increase in polysulfide chain length.

To correlate these derived polysulfide molecular structure with traditional Li-S battery environment, the DMSO solvent molecule were replaced with the popular Li-S battery electrolytes i.e. DOL and DME molecules in our DFT study. The lithium polysulfide molecule reacts similarly with DOL and DME system by mainly interacting with their oxygen, thereby shortening the Li-O bond (~1.92 Å) at the expense of elongated Li-S (2.40 Å) bond, The degree of DOL and DME electrolytes interaction with lithium depends on polysulfide chain length similar to the DMSO based molecular structure discussed above († Fig. S3). This validates our hypothesis that choice of DMSO as model system is suitable to study lithium polysulfide structure and solubility.

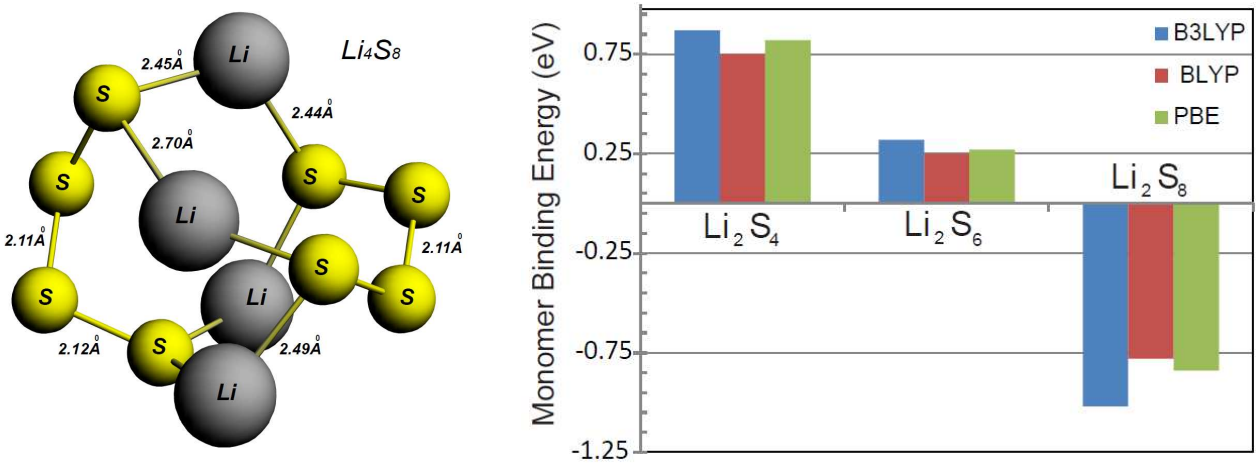

***Figure 2**. Molecular structure of Li_4S_8, dimer structure optimized using B3LYP-D3 with all electron TZ2P basis sets with the supramolecular setup (left). The binding energy difference between monomer and dimer units of lithium polysulfide species calculated using DFT with TZ2P basis set under different DFT functions (right).*

3.3 NMR Analysis of Polysulfide Species: We carried out ^{6}Li NMR measurements to investigate the lithium polysulfide molecules in solutions **A** and **B**. Figure 3a shows the ^{6}Li NMR resonance peak for both solutions **A** and **B** measured at room temperature at 11.7T magnetic field. A single sharp ^{6}Li NMR resonance peak at -0.5 and -0.6 ppm is observed for solutions **A** and **B,** respectively. The ^{6}Li NMR chemical shift is significantly different from the solid phase Li_2S_n (σ_{cs} > 0.5 ppm) and crystalline lithium sulfide (Li_2S, σ_{cs} ~ 0 ppm) phases[55]. This drastic change in the ^{6}Li NMR chemical shift implies that the molecular structure of dissolved polysulfide species is significantly different from its crystalline counterparts. Different lithium chemical environment in the dissolved polysulfide structure could be due

to solvent interactions as part of solvation phenomena. However, it is interesting to note a single ^{6}Li NMR resonance peak for each solution despite the possibility that our solutions might contain phase mixtures and dimer molecules as predicted by DFT analysis. A single resonance line suggests overlapping of ^{6}Li NMR chemical shifts from different phases of lithium polysulfide molecules (including the clustered phase), provided they all have a similar lithium environment. The optimized geometry of monomer units of lithium polysulfide molecules have very similar lithium environments such as Li-S bond (~2.53Å) and Li-O bond (~1.90Å) as shown in Figure 1. However, the dimer phase of lithium polysulfide shows wide variations in Li-S and Li-O bond lengths and hence is unlikely to have similar ^{6}Li NMR chemical shifts. To further verify this possibility, we calculated the NMR chemical shift († Fig. S3) of different phases of lithium polysulfide molecules using optimized molecular structures, which shows wide distribution (from -0.8 to -1.9 *ppm*) in contrast to the observed sharp ^{6}Li NMR line width (<0.1 *ppm*). In particular each lithium sites in dimer molecules has different chemical shift, that if present in the solution could lead to significant chemical shift distribution and subsequently broader line width (> 1 *ppm*). This is in agreement with MS analysis where only small (<3%) amount of Li_4S_8 dimer is observed and unlikely to be detected in our natural abundance ^{6}Li NMR.

Alternatively, the single ^{6}Li NMR resonance line observed might be due to fast exchange of lithium between different sites such as lithium polysulfide molecules and solvent molecules. This dynamics could lead to the chemically averaged single ^{6}Li NMR resonance provided the exchange rate is faster than NMR time scale (< *msec*). However, for dimer molecules (*i.e.* Li_4S_{2n}) such a fast exchange will be difficult as lithium is bridging species between two monomer units as shown in our DFT calculations (see Figure 2a). On the other hand, the lithium in the monomer species has more structural freedom for fast exchange with solvent molecule such as $Li_2S_n + 6DMSO \leftrightarrow 2(Li^+ - 3DMSO) + S_n^{2-}$. From our DFT structural analysis, it is evident that the DMSO molecule contains slightly negatively charged oxygen which strongly interacts with the lithium in the lithium polysulfide molecule. This interaction significantly increases the Li-S bond length indicating possible lithium exchange between the polysulfide solute and DMSO solvent molecules. To further verify this possibility, we calculated the ^{6}Li chemical shift of solvent bind lithium (DMSO-Li^+) which is about -1.0±0.2 *ppm* and in good agreement with observed peak position for both samples. In addition, our MS spectra is dominated by DMSO-Li^+ pairs and de-lithiated polysulfides S_6^{2-} in positive and negative ion modes respectively, providing robust evidence for the lithium bonding with solvent molecules as supported by our DFT calculations. These observations are in good agreement with a recent report by E. S. Shin and co-workers[56], where the lithium

exchange between solvent and polysulfide is proposed ($Li_2S_n \leftrightarrow 2Li^+ + S_n^{2-}$) and used to control its solubility through the *common ion effect*. It should be noted here that the dynamical lithium exchange mechanism described above is likely to be dependent on the chemical nature and concentration of the solvent environment.

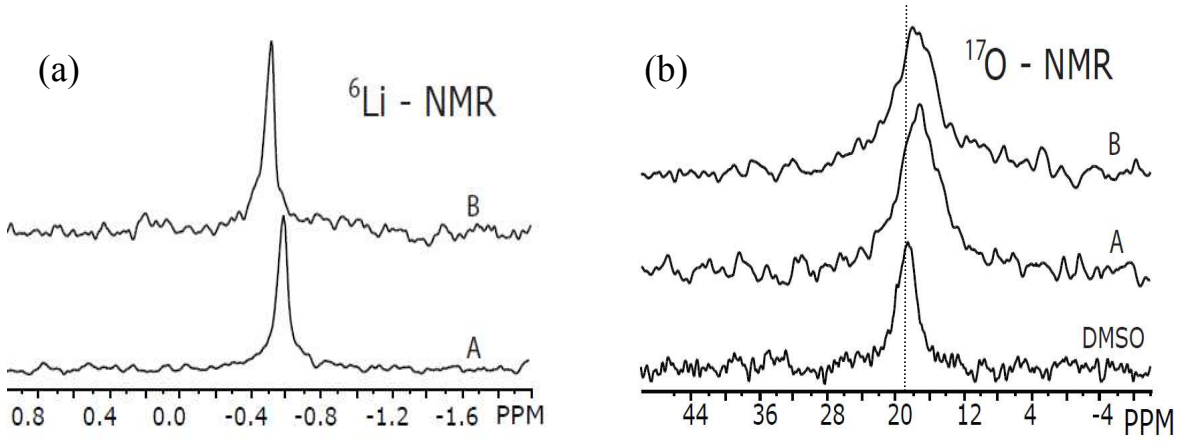

Figure 3. *a) ^{6}Li NMR peaks of pure DMSO solvent and lithium polysulfide solution **A** and **B** measured at 295K under 11.7T magnetic field. b) ^{17}O NMR peaks of pure DMSO solvent and lithium polysulfide solution **A** and **B** measured at 295K under 11.7T magnetic field.*

The dynamical lithium exchange picture can be further analyzed using ^{17}O NMR measurements. Figure 3b shows the measured natural abundance ^{17}O NMR of solutions **A** and **B** along with the pure DMSO solvent. Surprisingly both solutions **A** and **B** register a single ^{17}O NMR peak with slightly up field chemical shift (towards lower *ppm*) and nearly double the line width compared to the pure DMSO solvent. This line broadening and up field shift can be linked to the lithium exchange process between polysulfide solute and DMSO solvent molecule. Typically, such an exchange process induced changes in NMR parameters (*i.e.* chemical shift and line width) will depend on the rate of exchange, compositional ratio and chemical shift difference between the free and solvation bound DMSO solvent molecules. Our DFT calculations show that the ^{17}O chemical shift († Fig. S4) of lithium bonded DMSO molecules (2DMSO-Li^+) is 17 ± 1 *ppm* and slightly lower frequency (up field shift) compared with our calculations on the pure DMSO solvent (18.5 *ppm*). This is in agreement with the observed up field shift

(~1 *ppm*) of our dissolved polysulfide solutions (see Figure 3b). Overall, the lithium exchange process ($Li_2S_n \leftrightarrow 2Li^+ + S_n^{2-}$) is expected to produce de-lithiated polysulfide species (S_n^{2-}) and lithium bonded DMSO solvent molecules in the solution as observed in MS spectroscopic analysis discussed earlier. Combining the MS spectroscopic result with multinuclear NMR and computational analysis, it is evident that de-lithiated polysulfide species (S_n^{2-}) would be dominant species in the solution. Therefore, further structural and stability analysis will be focused on de-lithiated polysulfide species (S_n^{2-}).

3.4 XAS Analysis of Polysulfide species: Sulfur *K*-edge X-ray absorption near-edge structure (XANES) spectroscopy is a sensitive probe of the electronic and molecular structure of polysulfide molecules (S_n^{2-}). Figure 4 shows the normalized Sulfur K-edge XANES spectra for both polysulfide solutions **A** and **B** along with the pure DMSO solvent. A strong absorption peak near 2477 eV (peak 4) represents the DMSO solvent peak, whereas other low energy peaks (<2477 eV) represents polysulfide species. These low energy peaks around 2471 eV (peak 1), 2473 eV (peak 2) and 2474 eV (peak 3) are present for both solutions A and B, and it is difficult to assign these peaks to respective polysulfide species without calculations. To identify the specific polysulfide species in the Sulfur K-edge spectra, we calculated core-level XANES using the restricted excitation window (REW) linear-response TDDFT method[39,40]. As a first step, we calculated the XANES spectra for pure DMSO solvent which is in very good agreement with experimental spectra († Fig. S5). This validates our computational approach for core-level spectra and also provides the necessary reference to calculate energy shifts. We then calculated the XANES spectra for de-lithiated polysulfide ions (S_6^{2-} and S_3^{*-}) and lithium bonded DMSO molecules (2DMSO-Li^+) which are found to be the dominant species in our MS analysis. The de-lithiated polysulfide ion have clear signature peaks at low energy and matches the experimentally observed peaks 1 and 2. The lithium bonded DMSO molecular spectra are also very similar to the pure DMSO solvent spectrum, indicating that lithium binding only slightly perturbs the electronic structure of the DMSO molecule. This again confirms that the lithium interaction with DMSO mostly arises from electrostatic interactions between polarizable oxygen and lithium ions and might help drive the lithium exchange mechanism with the surrounding DMSO solvent molecules. This also suggests the presence of parent lithium polysulfide (Li_2S_n) molecules in the solution. Our calculated XANES spectra of Li_2S_n (n= 4, 6 & 8) with the supramolecular setup shows low energy peaks similar to the experimental peaks 1 and 3, respectively (Figure. 4). This result is in good agreement with recent experimental Sulfur K-edge analysis of solid state lithium polysulfide (Li_2S_n) molecules by L. Nazar et al[55]. By comparing the experimental and calculated XANES spectra, it is clear that our solutions containing the de-lithiated polysulfide species

(S_6^{2-}), lithium bonded DMSO solvent molecule (3DMSO-Li^+) and monomer lithium polysulfide species (Li_2S_n) and corroborates our initial MS analysis.

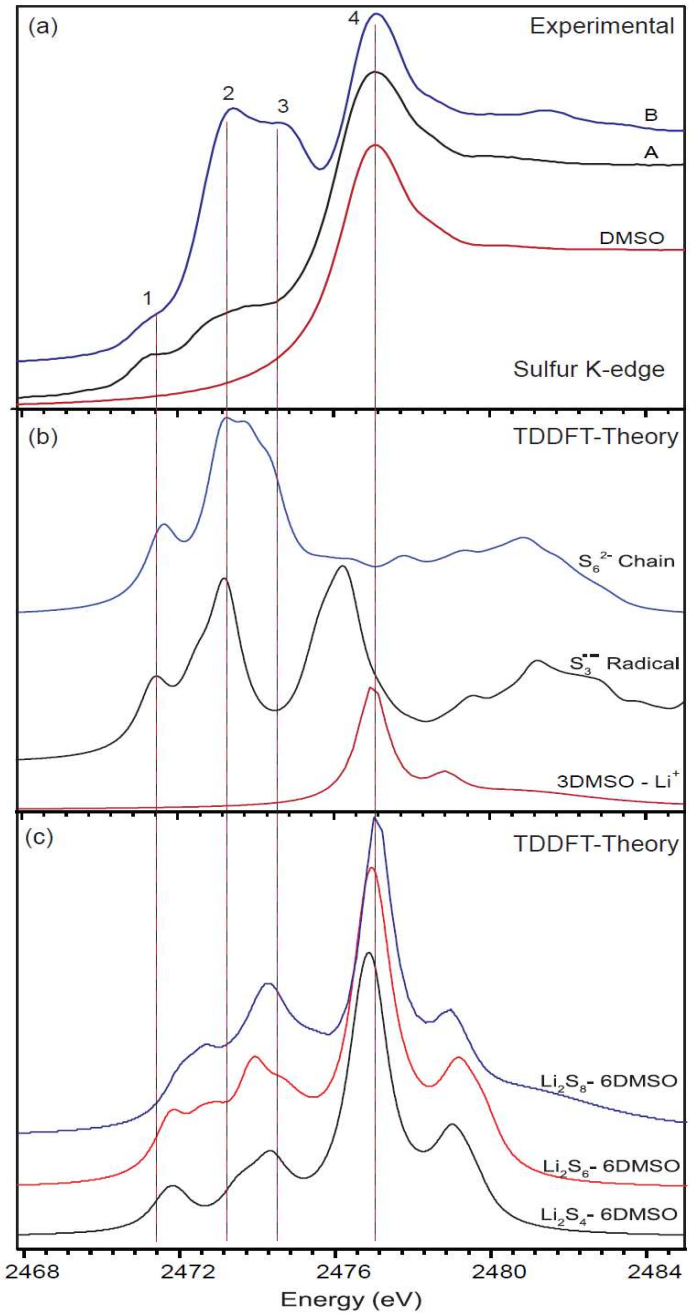

Figure 4. *(a) Sulfur K-edge XANES spectra of solution A and B along with pure DMSO solution. (b) Calculated XANES spectra of de-lithiated polysulfide ions (S_6^{2-} and S_3^{*-}) and lithium bind DMSO solvent (3DMSO-Li^+) (c) Calculated XANES spectra of the monomeric unit of lithium polysulfide molecule (Li_2S_n) with six explicit DMSO molecules as part of the solvation shell.*

3.5 Stability of Polysulfide ions: All our spectroscopic and computational studies suggest that de-lithiated polysulfide ions and in particular S_6^{2-} is the dominant species in the solution. The de-lithiated polysulfide ions (S_n^{2-}) could lead to free radical ions (such as, $S_4^{\bullet-}$, $S_3^{\bullet-}$ and $S_2^{\bullet-}$) through disproportion reactions ($S_n^{2-} \longrightarrow 2S_{n/2}^{\bullet-}$ and/or $S_n^{2-} \longrightarrow S_{n-x}^{\bullet-} + S_x^{\bullet-}$). In addition, these free radicals can be highly reactive with both the electrode and electrolyte materials of a battery and hence needs further analysis. The energetic requirements and kinetics for this disproportionation reaction to produce free radicals in the polysulfide ions are not well known. Therefore, we focused on studying the stability of polysulfide ions and corresponding energetics for disproportion reactions to produce free radicals in polysulfide solutions. ESR spectroscopy is used to identify and quantify of the free radical ions in the solution. Both solutions A and B show similar spectra features except the peak intensities. Figure 5 shows variable temperature X-band ESR spectra of solution B. The ESR spectra of both solutions **A** and **B** show similar spectra with a clear rhombic S=1/2 signature (g_x=2.0028, g_y=2.0333, g_z=2.0535 and g=2.0282) at low temperature (~125K) consistent with trisulfur $S_3^{\bullet-}$ free radicals reported in the literature[20, 57-59]. However, other free radicals such as $S_4^{\bullet-}$ and $S_2^{\bullet-}$ are not observed in the solution. The absence of $S_4^{\bullet-}$ radicals is not surprising considering the very low concentration of higher order polysulfide ions *i.e.* S_n^{2-} with *n*>6 in our solutions[34]. On the other hand, it is surprising to note the absence of $S_2^{\bullet-}$ radical, despite significant S_4^{2-} concentrations in the solutions. To analyze this further, we calculated the activation energy required for the possible disproportion reaction *i.e.* $S_4^{2-} \longrightarrow 2S_2^{\bullet-}$ from bonding energy differences between the reactant and product molecules. Our calculations predict a slightly exothermic reaction (~ -0.15 eV). Although, the formation of $S_2^{\bullet-}$ is slightly energetically favorable from a thermodynamics standpoint, the disproportionation of S_4^{2-} might need to overcome an energy barrier as shown in Figure 6. For example, to produce $S_2^{\bullet-}$ ions the S_4^{2-} ion has to undergo a bond breaking requiring thermal kinetics followed by state crossing from closed shell singlet to open shell doublet configuration. We therefore calculated the barrier to go from S_4^{2-} to the intermediate state $S_2^{-}...S_2^{-}$ on the singlet potential energy surface (see Figure 6). This will be the initial potential barrier for disproportion reaction of S_4^{2-} ion. This calculation yielded a high energy barrier of ~1.25 ± 0.05 eV and provides further evidence for the absence of $S_2^{\bullet-}$ radicals in our solutions. Similarly, the $S_2^{\bullet-}$ formation energy barrier under DOL/DME solvent system is ~1.40 ± 0.05 eV. On the other hand, despite the small concentration (~5 mM), the presence of $S_3^{\bullet-}$ free radicals

detected in ESR analysis confirms that S_6^{2-} ions undergo disproportion reaction $S_6^{2-} \longrightarrow 2S_3^{\bullet-}$ in DMSO solutions. Now we will focus on the possible energy requirement for such a disproportion reaction of S_6^{2-} ions.

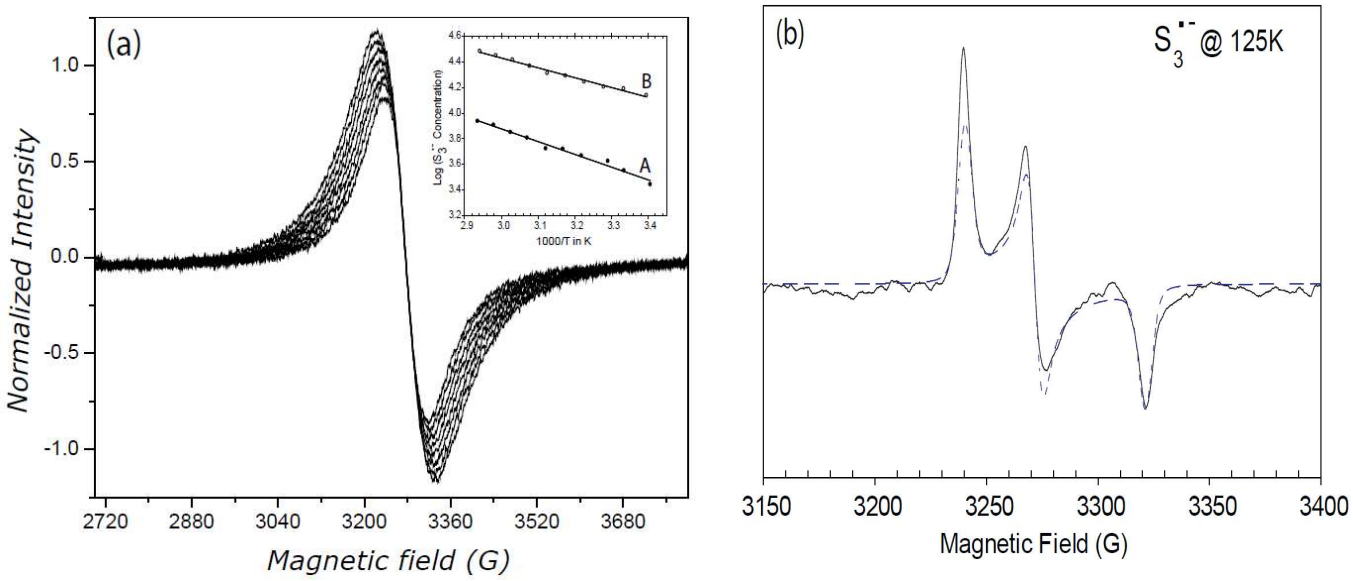

Figure 5. *a) Variable temperature ESR spectra of solution **B** showing the presence of $S_3^{\bullet-}$ free radical ions. The top inset shows the temperature dependent Arrhenius spectra of $S_3^{\bullet-}$ free radical ion concentration for both solutions **A** and **B**. b) The ESR spectra of solution **B** at 125K showing characteristic S=1/2 ESR spectra. The dotted line shows fitted ESR line which provides quantitative g tensor values and confirms the presence of $S_3^{\bullet-}$ radical ions.*

As shown in Figure 5a, the S=1/2 peaks are broadened due to thermally induced random motions at higher temperatures. It is interesting to note that the ESR peak integrals increases with increase in temperature and this phenomenon is completely reversible. The intensity of the ESR signal is directly related to the total concentration of the $S_3^{\bullet-}$ free radicals in the solution and can be used to analyze the thermal kinetics of the proposed disproportion reaction. The variable temperature ESR measurement reveals that with increase in temperature, the concentration of $S_3^{\bullet-}$ free radicals increases monotonically and exhibits Arrhenius-type behavior. This implies that the disproportionation reaction is a thermally activated process ($S_6^{2-} \xrightarrow{\Delta} 2S_3^{\bullet-}$) where the sulfur chains can split due to thermal kinetics. The activation energy calculated from temperature dependent $S_3^{\bullet-}$ free radicals concentration for both solutions are ~ 0.17 ± 0.05 eV. To further understand the disproportionation reaction ($S_6^{2-} \longrightarrow 2S_3^{\bullet-}$) we

performed DFT calculation and found that the reaction is slightly exothermic (~0.20 eV). Although, the $S_3^{\bullet-}$ is thermodynamically favorable, the thermally activated Arrhenius-type process observed for $S_3^{\bullet-}$ concentration indicates that the disproportionation of S_6^{2-} has to go through an energy barrier similar to S_4^{2-} discussed earlier. We calculated a barrier of ~0.25 ± 0.05 eV to form the intermediate state $S_3^- ... S_3^-$ (see Figure 7b). Similarly, the $S_3^{\bullet-}$ formation energy barrier under DOL/DME solvent system is ~0.40 ± 0.05 eV. This is about five times smaller compared with the barrier predicted for the $S_4^{2-} \longrightarrow S_2^- ... S_2^-$ discussed earlier (see Figure 6a). This low barrier is in good agreement with the activation energy (0.17 ± 0.05 eV) calculated from temperature dependent concentration of $S_3^{\bullet-}$ ions via ESR analysis.

This analysis suggests that dissolved S_6^{2-} polysulfide ions in an aprotic solvent can undergo disproportion reactions to produce highly reactive trisulfur $S_3^{\bullet-}$ free radicals. This free radical has also been recently detected in cycled Li-S batteries[20] and is likely to participate in the *shuttling phenomena* along with its parent S_6^{2-} molecule and cause parasitic reactions with the lithium anode during the extended cycling process. Incidentally, the trisulfur radical is well known and ubiquitous in many organic solutions and inorganic solids[60]. However, it is necessary to understand their chemical reactivity with electrolyte/electrode materials in sulfur based batteries so that they can be sequestered.

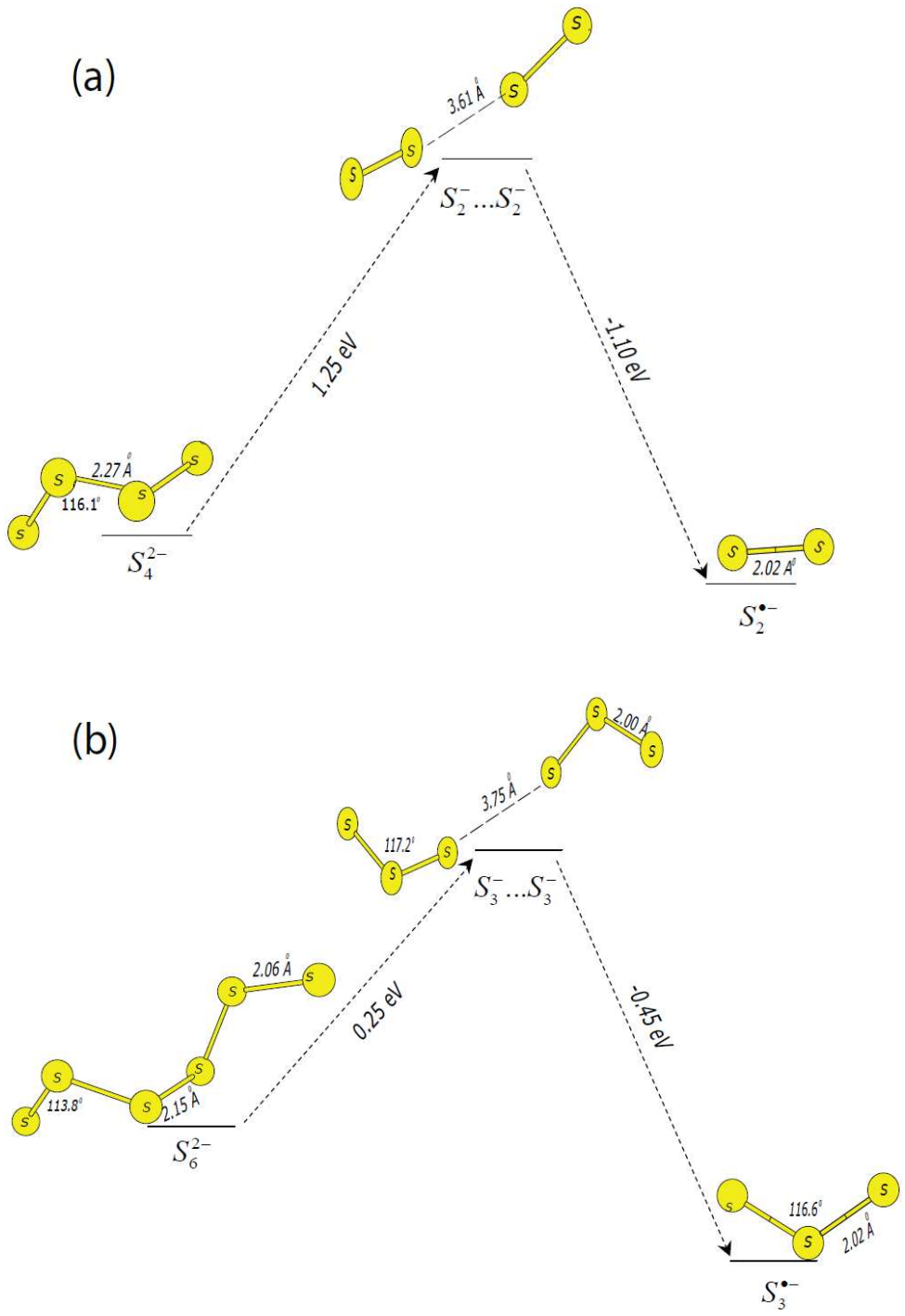

Figure 6. *Energy barrier of disproportionate reaction ($S_n^{2-} \longrightarrow 2S_{n/2}^{\bullet -}$) to produce a) $S_2^{\bullet -}$ free radical and b) $S_3^{\bullet -}$ free radical calculated using PBE-D3 with all electron TZ2P basis sets implemented in ADF 2013 package.*

3.6 Dissolution Mechanism: Based on our spectroscopic and theoretical analyses we can derive a possible dissolution mechanism for the lithium polysulfide species. The solubility is likely initiated by lithium exchange between polysulfide solute and solvent molecules. In particular, in higher-order lithium polysulfides (Li_2S_n ; $n \geq 6$) lithium exchange is more favored mainly due to their monomeric preference. In other words, higher-order lithium polysulfides are more soluble because the dissolution process could be viewed as the terminal lithium atoms engaging in rapid exchange with solvent molecules in a highly dynamical solvation shell. On the other hand, lower-order lithium polysulfides ($n<6$) favor dimerization, where lithium acts as bridge between monomer units and is not available to interact with the solvent molecules leading to relatively lower solubility. This hypothesis is supported by our XANES and ESR analyses as well as previous studies on the *common ion effect*[56], where lithium polysulfide solubility is decreased by increasing the lithium salt in the electrolyte (i.e. solvent system). In the *common ion effect*, the solvent system has sufficient lithium attached with active sites (for example, carbonyl oxygen) thereby limiting the lithium exchange process with lithium polysulfide molecules resulting in lower solubility. However, it should be noted that the preference for dimerization of lithium polysulfide molecules and the lithium exchange process depends highly on the nature of the solvent involved and thermal kinetics, respectively.

In a nutshell, solubility control requires careful design of the electrolyte system and one that is passive over an extended temperature and compositional window. To this end, our study suggests that an electrolyte system composed of non- coordinating anions (NCA) could be a better candidate for the Li-S battery. Indeed, ionic liquids consisting NCA such as bis(trifluoromethanesulfonyl)imide, bis(pentafluoroethanesulfonyl)amide, bis(fluorosulfonyl)amide and tetrafluoroborate were shown significant improvement in Li-S battery cycling performance[61]. Even further, an electrolyte system composed of weakly coordinating anions (WCA) such as fluorinated carborane based anions[62] could be a better candidate for the Li-S battery. The negative charge in these weakly coordinating anions are evenly distributed over the geometry of the molecule rather than at specific atomic site and will result in a relatively weaker electrostatic interaction with the lithium in the polysulfide molecules. Such WCA based electrolyte would reduce the solubility of polysulfide species and simultaneously increase the overall lithium conductivity of the cell.

4. Conclusion

We have studied the molecular structure and solubility of lithium polysulfide in an aprotic polar solvent medium using experimental and theoretical methods. Our DFT calculations predict that lower-order lithium polysulfide species (*i.e.* Li_2S_4) favor clustering or dimerization to form Li_4S_8 in the DMSO solvent system. Alternatively, higher-order species (*i.e.* Li_2S_6 and Li_2S_8) prefer monomeric units with lithium at both terminal ends of the chain structure. These terminal lithium ions can interact with polarizable sulfonyl oxygens of the DMSO solvent molecules and lead to lithium exchange between polysulfide species and DMSO solvent molecules in a highly dynamical solvation shell and initiates the dissolution process. Alternatively for the clustered or dimerized form of lithium polysulfide (*i.e.* Li_4S_8) the lithium acts as the bridging unit between two monomer polysulfide chains and is not available to interact with the surrounding DMSO molecules and results in lower solubility. Overall, the solvent interaction with lithium in polysulfide molecule is the crucial factor that controls solubility. For instance, an electrolyte system containing weakly coordinating anions could potentially reduce the solubility due to poor electrostatic interactions with lithium ions in the polysulfide molecule. Under the traditional electrolyte system with polarizable oxygen bonds, lithium exchange will initiate the dissolution process and lead to the *shuttling phenomena* of de-lithiated polysulfide ions. In particular, the ubiquitous S_6^{2-} polysulfide ions can undergo disproportion reactions thereby producing highly reactive $S_3^{\bullet-}$ radical ions in the solution. Based on our analyses, the *shuttling phenomena* observed in Li-S batteries is likely to include $S_3^{\bullet-}$ radical ions which can cause parasitic reactions with the lithium anode. Efforts to sequester these radical ions would require more detailed studies.

Acknowledgements

We thank Drs. *Karl T. Mueller* and *Jianzhi Hu* for their support and fruitful discussions. The research described in this paper is part of the *Chemical Imaging Initiative* led by Dr. *Lou Terminello* at Pacific Northwest National Laboratory (PNNL). It was conducted under the Laboratory Directed Research and Development Program at PNNL, a multi-program national laboratory operated by Battelle under Contract DE-AC05-76RLO1830 for the U.S. Department of Energy (DOE). The synthesis part of this work is supported by the *Joint Center for Energy Storage Research* (JCESR), an Energy Innovation Hub funded by the U.S. Department of Energy, Office of Science, Basic Energy Sciences (BES). The NMR, MS and DFT computation work was carried out at EMSL (www.emsl.pnl.gov), a national scientific user facility sponsored by the DOE's Office of Biological and Environmental Research. The XAS analysis were

performed at National Synchrotron Light Source (NSLS) a national scientific user facility sponsored by the BES.

Notes and references

Pacific Northwest National Laboratory, Richland, WA 99352, USA.
** Corresponding Author, Email: Vijay@pnnl.gov ; Ph: +1-509-371-6540*

† Electronic Supplementary Information (ESI) available. [Mass Spectrometry spectra, DFT calculated NMR chemical shifts and XANES spectra of pure DMSO]. See DOI: 10.1039/b000000x/

1. X. Ji and L. F. Nazar, *Journal of Materials Chemistry*, 2010, **20**.
2. Y. Yang, G. Zheng and Y. Cui, *Energy & Environmental Science*, 2013, **6**, 1552-1558.
3. P. G. Bruce, S. A. Freunberger, L. J. Hardwick and J.-M. Tarascon, *Nat Mater*, 2012, **11**, 19-29.
4. A. Manthiram, Y. Fu and Y.-S. Su, *Accounts of Chemical Research*, 2012.
5. B. Ding, C. Yuan, L. Shen, G. Xu, P. Nie and X. Zhang, *Chemistry-a European Journal*, 2013, **19**, 1013-1019.
6. X. Ji, K. T. Lee and L. F. Nazar, *Nat Mater*, 2009, **8**, 500-506.
7. M. Xiao, M. Huang, S. Zeng, D. Han, S. Wang, L. Sun and Y. Meng, *Rsc Advances*, 2013, **3**, 4914-4916.
8. Y. Yang, G. Zheng and Y. Cui, *Chemical Society Reviews*, 2013, **42**, 3018-3032.
9. Y. Diao, K. Xie, S. Xiong and X. Hong, *Journal of Power Sources*, 2013, **235**, 181-186.
10. S. S. Zhang, *Journal of Power Sources*, 2013, **231**, 153-162.
11. S. S. Zhang, *Electrochimica Acta*, 2013, **97**, 226-230.
12. Y.-S. Su and A. Manthiram, *Nature Communications*, 2012, **3**.
13. C. Zu, Y.-S. Su, Y. Fu and A. Manthiram, *Physical Chemistry Chemical Physics*, 2013, **15**, 2291-2297.
14. L. Ji, M. Rao, H. Zheng, L. Zhang, Y. Li, W. Duan, J. Guo, E. J. Cairns and Y. Zhang, *Journal of the American Chemical Society*, 2011, **133**, 18522-18525.
15. M.-K. Song, Y. Zhang and E. J. Cairns, *Nano Letters*, 2013, **13**, 5891-5899.
16. X. Liang, Z. Wen, Y. Liu, M. Wu, J. Jin, H. Zhang and X. Wu, *Journal of Power Sources*, 2011, **196**, 9839-9843.
17. S. S. Zhang, *Electrochimica Acta*, 2012, **70**, 344-348.
18. X. Ji, S. Evers, R. Black and L. F. Nazar, *Nat Commun*, 2011, **2**, 325.
19. M.-K. Song, E. J. Cairns and Y. Zhang, *Nanoscale*, 2013, **5**, 2186-2204.
20. C. Barchasz, F. Molton, C. Duboc, J.-C. Leprêtre, S. Patoux and F. Alloin, *Analytical Chemistry*, 2012, **84**, 3973-3980.
21. M. Hagen, P. Schiffels, M. Hammer, S. Dörfler, J. Tübke, M. J. Hoffmann, H. Althues and S. Kaskel, *Journal of The Electrochemical Society*, 2013, **160**, A1205-A1214.
22. Y. Diao, K. Xie, S. Xiong and X. Hong, *Journal of The Electrochemical Society*, 2012, **159**, A421-A425.
23. L. Wang, T. Zhang, S. Yang, F. Cheng, J. Liang and J. Chen, *Journal of Energy Chemistry*, 2013, **22**, 72-77.
24. T. Yim, M.-S. Park, J.-S. Yu, K. J. Kim, K. Y. Im, J.-H. Kim, G. Jeong, Y. N. Jo, S.-G. Woo, K. S. Kang, I. Lee and Y.-J. Kim, *Electrochimica Acta*, 2013, **107**, 454-460.
25. J. Gao, M. A. Lowe, Y. Kiya and H. D. Abruña, *The Journal of Physical Chemistry C*, 2011, **115**, 25132-25137.
26. W. Wang, Y. Wang, Y. Huang, C. Huang, Z. Yu, H. Zhang, A. Wang and K. Yuan, *J Appl Electrochem*, 2010, **40**, 321-325.
27. L. Suo, Y.-S. Hu, H. Li, M. Armand and L. Chen, *Nat Commun*, 2013, **4**, 1481.
28. R. D. Rauh, F. S. Shuker, J. M. Marston and S. B. Brummer, *Journal of Inorganic and Nuclear Chemistry*, 1977, **39**, 1761-1766.
29. N. S. A. Manan, L. Aldous, Y. Alias, P. Murray, L. J. Yellowlees, M. C. Lagunas and C. Hardacre, *The Journal of Physical Chemistry B*, 2011, **115**, 13873-13879.

30. Y. V. Mikhaylik and J. R. Akridge, *Journal of The Electrochemical Society*, 2004, **151**, A1969-A1976.
31. W. F. Giggenbach, *Inorganic Chemistry*, 1974, **13**, 1724-1730.
32. W. Giggenbach, *Inorganic Chemistry*, 1972, **11**, 1201-1207.
33. I. Filpponen, A. Guerra, A. Hai, L. A. Lucia and D. S. Argyropoulos, *Industrial & Engineering Chemistry Research*, 2006, **45**, 7388-7392.
34. E. Levillain, P. Leghie, N. Gobeltz and J. P. Lelieur, *New J. Chem.*, 1997, **21**, 335-341.
35. R. Steudel and Y. Steudel, *Chemistry – A European Journal*, 2013, **19**, 3162-3176.
36. S. Licht and J. Davis, *The Journal of Physical Chemistry B*, 1997, **101**, 2540-2545.
37. G. te Velde, F. M. Bickelhaupt, E. J. Baerends, C. Fonseca Guerra, S. J. A. van Gisbergen, J. G. Snijders and T. Ziegler, *Journal of Computational Chemistry*, 2001, **22**, 931-967.
38. S. Grimme, J. Antony, S. Ehrlich and H. Krieg, *The Journal of Chemical Physics*, 2010, **132**, 154104-154119.
39. A. D. Becke, *Physical Review A*, 1988, **38**, 3098-3100.
40. C. Lee, W. Yang and R. G. Parr, *Physical Review B*, 1988, **37**, 785-789.
41. S. Grimme, W. Hujo and B. Kirchner, *Physical Chemistry Chemical Physics*, 2012.
42. M. Valiev, E. J. Bylaska, N. Govind, K. Kowalski, T. P. Straatsma, H. J. J. Van Dam, D. Wang, J. Nieplocha, E. Apra, T. L. Windus and W. A. de Jong, *Computer Physics Communications*, 2010, **181**, 1477-1489.
43. K. Lopata, B. E. Van Kuiken, M. Khalil and N. Govind, *Journal of Chemical Theory and Computation*, 2012, **8**, 3284-3292.
44. Y. Zhang, J. D. Biggs, D. Healion, N. Govind and S. Mukamel, *The Journal of Chemical Physics*, 2012, **137**, -.
45. B. E. Van Kuiken, M. Valiev, S. L. Daifuku, C. Bannan, M. L. Strader, H. Cho, N. Huse, R. W. Schoenlein, N. Govind and M. Khalil, *The Journal of Physical Chemistry A*, 2013, **117**, 4444-4454.
46. D. Healion, Y. Zhang, J. D. Biggs, N. Govind and S. Mukamel, *The Journal of Physical Chemistry Letters*, 2012, **3**, 2326-2331.
47. P. Nichols, N. Govind, E. J. Bylaska and W. A. de Jong, *Journal of Chemical Theory and Computation*, 2009, **5**, 491-499.
48. E. van Lenthe, E. J. Baerends and J. G. Snijders, *The Journal of Chemical Physics*, 1994, **101**, 9783-9792.
49. T. Noro, Quantum chemistry group, Sapporo, Japan, http://setani.sci.hokudai.ac.jp/sapporo, 2013, vol. 2013.
50. T. Noro, M. Sekiya and T. Koga, *Theor Chem Acc*, 2012, **131**, 1-8.
51. EMSL, https://bse.pnl.gov/bse/portal, 2013, vol. 2013.
52. K. L. Schuchardt, B. T. Didier, T. Elsethagen, L. Sun, V. Gurumoorthi, J. Chase, J. Li and T. L. Windus, *Journal of Chemical Information and Modeling*, 2007, **47**, 1045-1052.
53. A. D. Becke, *The Journal of Chemical Physics*, 1993, **98**, 1372-1377.
54. B. Meyer, *Chemical Reviews*, 1976, **76**, 367-388.
55. M. Cuisinier, P.-E. Cabelguen, S. Evers, G. He, M. Kolbeck, A. Garsuch, T. Bolin, M. Balasubramanian and L. F. Nazar, *The Journal of Physical Chemistry Letters*, 2013, **4**, 3227-3232.
56. E. S. Shin, K. Kim, S. H. Oh and W. Il Cho, *Chemical Communications*, 2013, **49**, 2004-2006.
57. S. D. McLaughlan and D. J. Marshall, *The Journal of Physical Chemistry*, 1970, **74**, 1359-1363.
58. L. Bonazzola, J. P. Michaut and J. Roncin, *The Journal of Chemical Physics*, 1985, **83**, 2727-2732.
59. J. Goslar, S. Lijewski, S. K. Hoffmann, A. Jankowska and S. Kowalak, *The Journal of Chemical Physics*, 2009, **130**, 204504.
60. T. Chivers and P. J. W. Elder, *Chemical Society Reviews*, 2013, **42**, 5996-6005.
61. J.-W. Park, K. Ueno, N. Tachikawa, K. Dokko and M. Watanabe, *The Journal of Physical Chemistry C*, 2013, **117**, 20531-20541.
62. S. H. Strauss, *Chemical Reviews*, 1993, **93**, 927-942.

